

Quaking in Soft Granular Particles with Speed-dependent Friction: Role of Critical Volume Fraction and Inertia

Wei-Chang Lo, Jih-Chiang Tsai

Institute of Physics, Academia Sinica, Taipei, 115201, Taiwan

Abstract

Our previous numerical simulation [C.-E. Tsai et al., *Physical Review Research* **6**, 023065 (2024)] has shown that, for soft granular particles under quasistatic shearing, incorporating a speed-dependent friction is essential to reproduce the rate-dependent stick-slip fluctuations that have been found in the laboratory experiment [J.-C. Tsai et al., *Physical Review Letters* **126**, 128001 (2021)]. As a continuation, here we employ the simulation in a wide range of driving speeds to examine the role of grain inertia in the quaking dynamics. With our Stribeck-Hertz model, we find that having the volume fraction exceeding a critical value ϕ_c is a necessary condition for the quaking to occur, and that the value of ϕ_c is determined by material parameters only, independent of the driving rate. The effect of grain inertia generally suppresses the occurrence of quaking, and we conclude by presenting the state diagrams which exhibit a progressive narrowing of the quaking regime as the driving speed increases and the disappearance of quaking at an extremely high shear rate.

Keywords: granular materials, slip avalanches, inertial rheology

1. Introduction

Various seismological views on the mechanisms of earthquake and fault dynamics have progressively developed in the past century, including the recognition of fractality at the fault zone and granular aspects of earthquake and fault dynamics [1]. Therefore, the intermittent dynamics (e.g. slip avalanches) in granular materials has been extensively investigated to

inspect whether it reproduces the scale-invariant power laws in seismology [2–7]. A great deal of such studies were performed using dry granular particles. However, fluid content at the fault zone is one of the main factors that leads to deviation of magnitude-frequency distributions from the seminal Gutenberg-Richter law [1, 8]. Meanwhile, there is evidence that faults are lubricated during earthquakes [9]. Velocity weakening in fault gouge and in induced earthquakes via fluid injection have also been reported [10–12]. These works have raised our interest into the effect of lubrication upon the intermittency in a sheared granular material.

We previously conducted a laboratory experiment of granular shear flow with an interstitial fluid that exhibited strong intermittency, characterized by bursts of grain-level displacement and sudden release of stresses only in the mid-range of the driving rates [13]. To understand this intriguing rate dependence, we have also investigated the tribology between surfaces of these granular particles immersed in the same fluid [14]: The time averaged friction force shows a nonmonotonic dependence on the sliding speed between the particles that is consistent with the paradigmatic Stribeck diagram [15, 16]. More specifically, at low speeds, we have identified an onset value V_c beyond which the friction between particles begins to reduce, presumably due to the lubrication of the interstitial fluid. Based on these empirical facts, we have also set up a numerical simulation [17] to demonstrate that, for a granular packing under continuous shearing, the speed-dependent friction is not only a sufficient but also a necessary condition for the sudden changes of several physical quantities, including the coordination number, the elastic energy, and the boundary stress. Collectively, we call these sudden changes *quaking* for its resemblance to earthquakes. In the simulation, we have used a dimensionless parameter called the *slipperiness*, $\dot{\gamma}d/V_c$, as one of the main control parameters (in addition to the volume fraction ϕ). Here, the physical shear rate is defined as $\dot{\gamma} \equiv U/Z_0$, where U is the driving speed, Z_0 is the thickness of the granular packing, d stands for the mean diameter of particles and V_c for the aforementioned onset speed of the velocity weakening.

In our previous work [17], in order to focus on quasistatic flows, U was limited to a low value (0.1 cm/s). Several decades of changes in the value of $\dot{\gamma}d/V_c$ were achieved by varying the material parameter V_c hypothetically. However, a more natural, real-world like approach should have been maintaining the material parameter V_c and varying the driving speed U instead. One important motivation of the present work is to go beyond the quasistatic limit and understand whether increasing the driving speed U and, in turn,

bringing in the effect of inertia would change the quaking dynamics.

Going beyond the quasistatic limit also means the substantial reduction of packing densities below the critical point of transition. In the present work, we locate the critical points of transition in the steady-shear dynamics, and use these critical points as the baseline to compare models with or without speed-dependent friction.

2. Methodology

2.1. Numerical setup

As in our previous work, our simulations are carried out in LAMMPS [18]—please see Ref. [17] for details of our simple-shear geometry, the binary mixture of soft spheres in two diameters ($0.9d_w$ and $1.1d_w$, in which d_w stands for the diameter of particles constituting the driving walls) with fixed number for both, the driving walls moving along $\pm X$ directions at a constant velocity $\pm U/2$ and a fixed separation Z_0 for each target volume fraction, the periodic boundary conditions in the direction of X and Y , and the material parameters (elastic moduli and mass) mimicking our laboratory experiment [13]. Here we merely describe the essentials. In most cases, we make a side-by-side comparison between the results from two models as follows:

1. The Coulomb-Hertz (CH) model, also known as the “history-dependent Hertz model” in LAMMPS’ documentation [19]. In this model, particles i and j interact viscoelastically via the *overlap distance* $\delta_{ij} = R_i + R_j - r_{ij}$ as the strain of deformation, where R_i and R_j are the particle radii, and r_{ij} is the separation between the centers of these two particles; note that $\delta_{ij} \equiv 0$ if $r_{ij} > R_i + R_j$. In the normal direction, the force \mathbf{f}_N^{ij} follows the law of a Hertzian contact with a viscous damping:

$$\mathbf{f}_N^{ij} = \sqrt{\delta_{ij} R_{\text{eff}}} (K_N \delta_{ij} \hat{\mathbf{n}}_{ij} - m_{\text{eff}} \gamma_N \mathbf{v}_N^{ij}), \quad (1)$$

where R_{eff} , m_{eff} , \mathbf{v}_N^{ij} and $\hat{\mathbf{n}}_{ij}$ are the effective radius, the effective mass, the normal component of the relative velocity and the unit vector along the line connecting the centers of the two particles, respectively, and K_N is the elastic constant and γ_N is the viscoelastic damping constant for normal contact, respectively [19]. In the tangential direction, the force without damping,

$$\mathbf{f}_T^{ij} = -\sqrt{\delta_{ij} R_{\text{eff}}} K_T \Delta \mathbf{S}_T^{ij}, \quad (2)$$

grows linearly with the lateral movement between particle surfaces $\Delta \mathbf{S}_T^{ij}$ since the moment of contact, up to the saturation magnitude $f_T^{ij} = \mu_0 f_N^{ij}$, until the two spheres fall apart, i.e., $\delta_{ij} = 0$. The Coulomb coefficient μ_0 and the elastic constant for tangential contact K_T are both material constants that are independent of particle movement. In this work, we set $K_N = K_T = 1.5$ MPa, and $\gamma_N = 1.5 \times 10^5$ (cm·s)⁻¹ by default unless otherwise specified. The choice of these parameters is based on the previous experimental characterization of the PDMS spheres [13].

2. The Stribeck-Hertz (SH) model. The interparticle force laws are the same as the CH model except a slight modification: To replicate the velocity weakening reported in Ref. [14], we replace the constant μ_0 with a speed-dependent friction coefficient

$$\mu(v_T) = \begin{cases} \mu(0) & \text{if } v_T \leq V_c \\ \mu(0) \times (v_T/V_c)^{-1} & \text{if } v_T > V_c, \end{cases} \quad (3)$$

where v_T stands for the sliding speed between two particles when they are overlapping, that is, the magnitude of time derivatives of $\Delta \mathbf{S}_T^{ij}$, and V_c is a material-specific characteristic speed that corresponds to the onset of the velocity weakening. As a continuation of our previous work, the other material-specific constant $\mu(0)$ is set to unity.

2.2. Identifying the critical volume fraction

Since the magnitude of the tangential force in the SH model is capped at $f_T^{ij} = \mu(v_T) f_N^{ij}$, and $\mu(v_T)$ is floating according to the magnitudes of v_T and V_c , the maximum of f_T^{ij}/f_N^{ij} is now floating as well. In other words, the distribution of f_T^{ij}/f_N^{ij} mixes (i) those are yet to reach the threshold $\mu(0)$ and (ii) those are weakened down to $\mu(0) \times (v_T/V_c)^{-1}$. Measuring f_T^{ij}/f_N^{ij} or the (global) stress ratio would not necessarily reflect the actual interparticle friction coefficient, which is a crucial quantity for examining the dynamics of granular flows. Hence, we aim to circumvent this issue and adopt an experimentally accessible approach to investigate the dynamics governed by the SH model.

Generally speaking, the dynamics of granular particles under an imposed shear is controlled by the volume fraction ϕ and the shear rate $\dot{\gamma}$. These granular particles start to form a network of enduring contacts as the volume fraction ϕ reaches a critical value ϕ_c [20, 21]. For infinitely rigid spheres,

ϕ_c corresponds to the jamming point [22, 23]. For soft particles, on the other hand, a volume fraction beyond ϕ_c is accessible. With the increased volume fraction, the deformation at the contacts become progressively persistent and dominate the rheological responses. The critical point ϕ_c has been used as the reference of transition in comparing the rheology of debris flow samples [24]. Specifically, the critical volume fraction of soft granular particles represents a regime transition between collisional flows ($\phi < \phi_c$) and elastoplastic deformation ($\phi > \phi_c$); the former exhibits a dominant effect of particle inertia, and the latter is considered quasistatic [25]. It is expected that the granular dynamics governed by the CH or the SH model would exhibit substantial differences only when $\phi > \phi_c$, such that the role of interparticle friction becomes significant because of the enduring overlaps.

A number of ways to locate ϕ_c of soft particles have been discussed in the literature; see Ref. [26] and the references therein. In general, these methods usually involve identifying the diverged fluctuations that are associated with building up the contact network by increasing ϕ . Here we choose to look into the fluctuation of the coordination number $Z(t)$, which is the contact numbers per particle averaged over all particles (excluding the wall particles) at time t . For each value of ϕ , the fluctuation of the coordination number is represented by the standard deviation $\xi_Z(\phi) = \sqrt{\sum_{\ell=1}^n [Z(\phi, t_\ell) - \bar{Z}]^2 / (n - 1)}$, where \bar{Z} is the mean of $Z(\phi, t_\ell)$, t_ℓ is the sampled time point and n is the number of samples. In other words, ξ_Z estimates the spread of the contact number of individual particles relative to the mean of the population packed and sheared at a given volume fraction ϕ . Figure 1 shows a drastic increase of ξ_Z around a narrow range of ϕ in most of the examples. We thus calculated the finite difference of ξ_Z and interpolated where the slope changed sign as the critical volume fraction ϕ_c , indicated by the vertical dashed lines in Fig. 1.

3. Main Results

3.1. Critical volume fraction depending on material parameters

Figure 2(a) reproduces the well known fact that the critical volume fraction ϕ_c in the conventional (CH) model drops monotonically with the increasing value of μ_0 . It has been reported that the values of ϕ_c depend on μ_0 but not on the shear rate $\dot{\gamma}$ [25]. These values are also confined by two previously reported limits: $\phi_c \approx 0.64$ while $\mu_0 \rightarrow 0$, and $\phi_c \approx 0.55$ while $\mu_0 \rightarrow \infty$ [26].

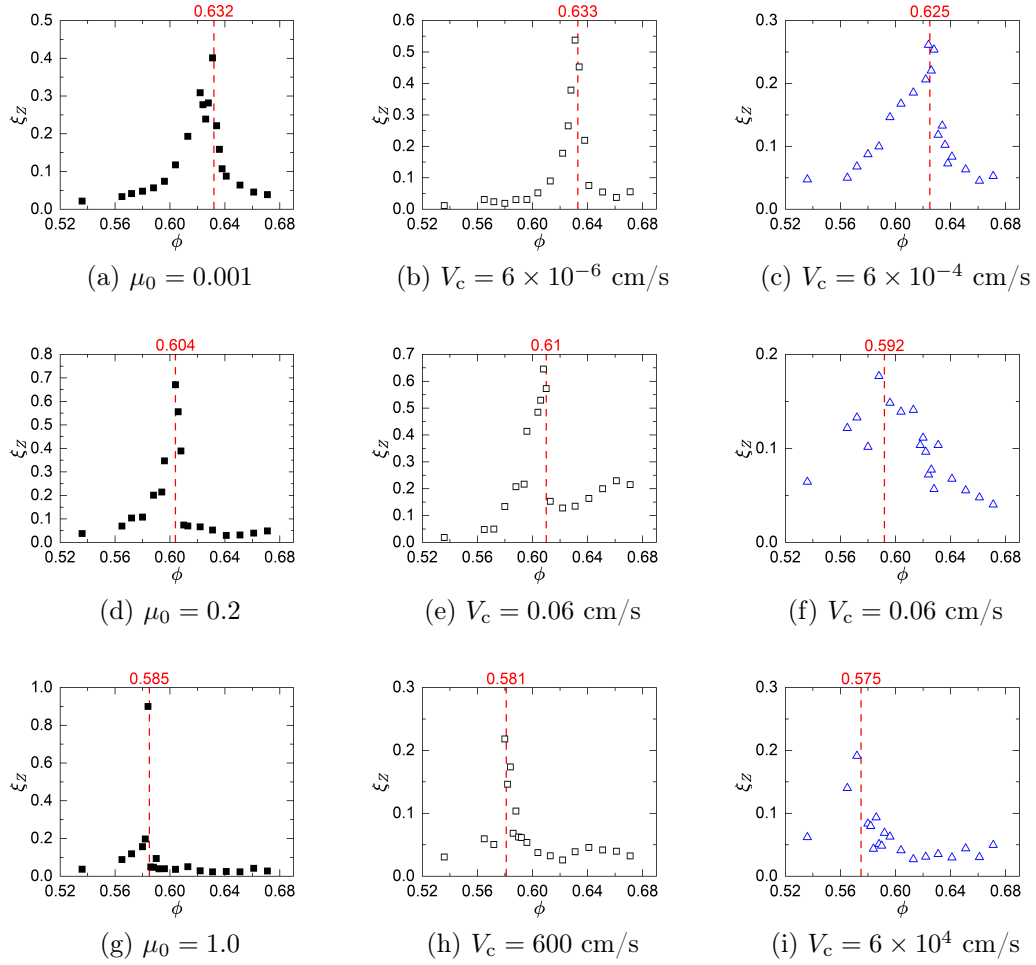


Figure 1: Nine examples of the fluctuation of coordination numbers ξ_Z that varies with the volume fraction ϕ , and with various Coulomb coefficients μ_0 (the CH model) or weakening onset speeds V_c (the SH model). The left column shows examples from the CH model. The middle and the right columns show examples from the SH model with $U = 0.01$ cm/s and $U = 1.0$ cm/s, respectively. The vertical dashed line indicates the value of the critical volume fraction for each panel.

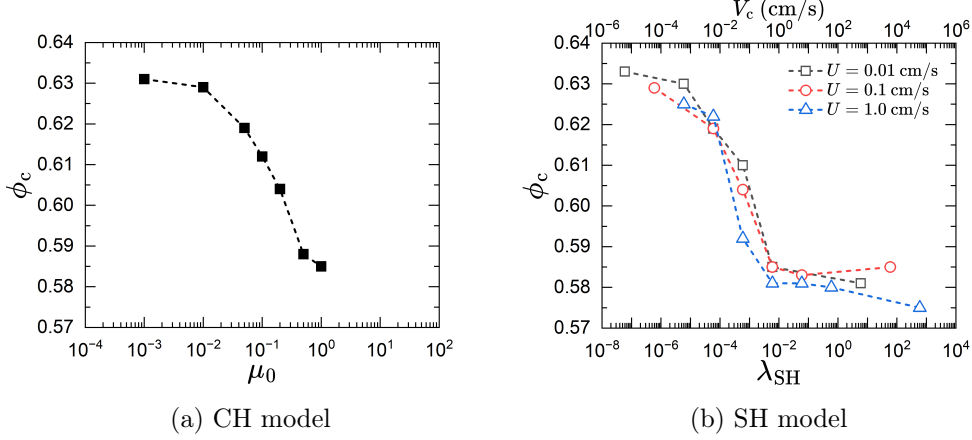


Figure 2: The critical volume fraction ϕ_c versus material-specific parameters. (a) ϕ_c versus the Coulomb coefficient μ_0 in the CH model, with $U = 0.1$ cm/s. (b) ϕ_c versus a new dimensionless parameter, $\lambda_{SH} = m\gamma_N V_c / K_N d$, with three different driving speeds. In these simulations, $K_N = 1.5$ MPa and $\gamma_N = 1.5 \times 10^5$ (cm·s) $^{-1}$ were fixed, and we varied λ_{SH} by changing V_c .

Interestingly, in our SH model, Fig. 2(b) shows that the value of ϕ_c is also monotonically dependent on the material-specific parameter V_c but not sensitive to the change of driving speed U by two orders of magnitude. The trend of ϕ_c in Fig. 2(b) are consistent with two *trivial* limits. For $V_c \rightarrow \infty$, the particles are never weakened thus $\mu(v_T) = \mu(0) = 1$; in this limit ϕ_c should be the same as $\mu_0 = 1$ in the CH model, i.e., the rightmost point in Fig. 2(a) where $\phi_c = 0.585$. On the other hand, when $V_c \rightarrow 0$, even the slightest sliding shall trigger the weakening, and the particles behave like they are frictionless; in this limit, ϕ_c should be asymptotically approaching 0.64, but the minimal V_c and the driving speeds we have tested lead to ϕ_c close to that corresponding to $\mu_0 = 0.001$ in the CH model, i.e., the leftmost point in Fig. 2(a) where $\phi_c = 0.632$.

The dependence on the material parameters shown in Fig. 2(b) can be nondimensionalized as we define $\lambda_{SH} \equiv m\gamma_N V_c / K_N d$, where m is the mean mass of the particles. We may interpret λ_{SH} as a ratio of the retardation time $\tau_R = m\gamma_N / K_N$ to the critical weakening time $\tau_c = d / V_c$. The sliding velocity between two colliding particles is coupled with how long they stay overlapped while increasing the tangential displacement $\Delta \mathbf{S}_T^{ij}$ in Eq. (2). Hence, λ_{SH} can be seen as a measure of whether the duration of interparticle sliding while

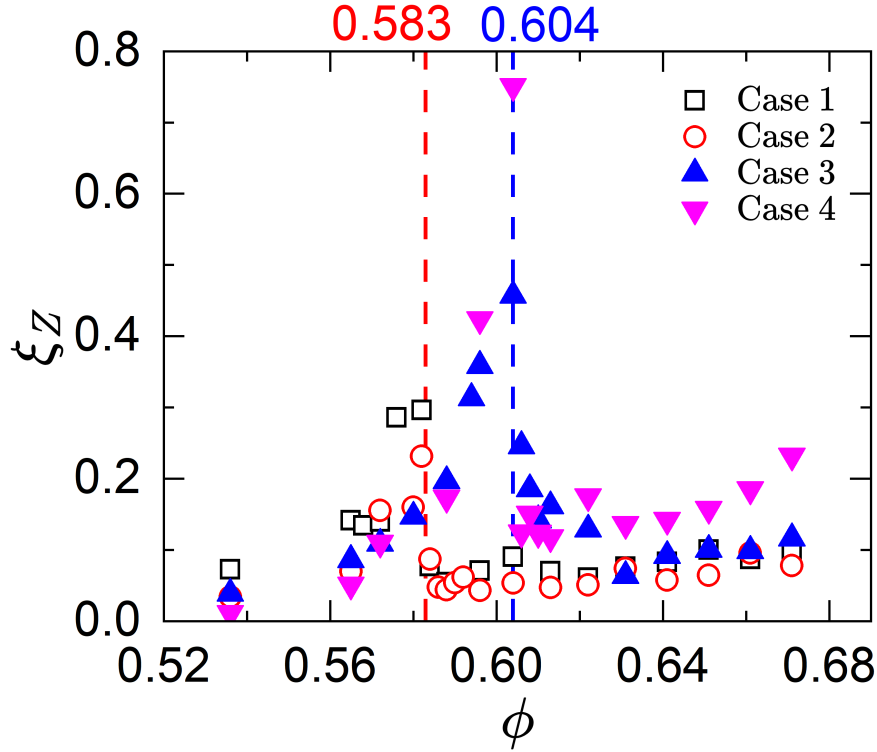


Figure 3: Simulations governed by the SH model with $\lambda_{\text{SH}} = 6 \times 10^{-2}$ (Case 1 and 2) and $\lambda_{\text{SH}} = 6 \times 10^{-4}$ (Case 3 and 4) are characterized by $\phi_c = 0.583$ and $\phi_c = 0.604$, respectively. Note that these simulations had various combination of parameters as shown in Table 1.

Case	V_c (cm/s)	K_N (MPa)	γ_N (cm·s) $^{-1}$	λ_{SH}
1	0.6	0.15	1.5×10^5	6×10^{-2}
2	6.0	1.5	1.5×10^5	6×10^{-2}
3	0.06	1.5	1.5×10^5	6×10^{-4}
4	0.006	15.0	1.5×10^7	6×10^{-4}

Table 1: Parameters used in the simulations that are plotted in Fig. 3.

transiently overlapping is short enough to trigger the velocity weakening; the physical meaning of λ_{SH} will be further elaborated in Sec. 4.

To show the validity of ϕ_c being a function of λ_{SH} , we plot the fluctuation of coordination numbers ξ_Z of four examples with varied parameters V_c , K_N and γ_N that correspond to two different values of λ_{SH} (Table 1) in Figure 3. It is evident that various combination of these parameters which correspond to the same value of λ_{SH} will result in the same value of ϕ_c .

Overall, ϕ_c as a function of λ_{SH} in Fig. 2(b) qualitatively resemble those as a function of μ_0 in Fig. 2(a). The value of ϕ_c offers a convenient basis for comparing simulations governed by the CH and the SH models. Given that the values of ϕ_c for the CH model and for the SH model are both material-specific and insensitive to the driving speed, we speculate that there would be a mapping between the dynamics governed by the CH and the SH model via the distance to a similar value of ϕ_c . We then will have a convenient baseline to group the data from both models to make side-by-side comparisons. In the following two subsections, detailed comparisons are made based on the choice of material parameters with which both models share a similar value of ϕ_c .

3.2. Verifying universal behaviors disclosed by the distance to ϕ_c

The steady-state dynamics governed by both models, at various shear rates tested in our simulations, quantitatively falls into *two* distinct regimes based on the difference between ϕ and ϕ_c : collisional flows ($\phi < \phi_c$) and quasistatic flows ($\phi > \phi_c$). Each regime features a certain scaling law between variables, for instance, the normal stress and the shear rate [21, 25].

In each panel of Fig. 4, we include two sets of simulations for both models, each of which contains data either above or below a similar value of ϕ_c , i.e., $\phi_c = 0.630 \pm 0.001$ and 0.585 ± 0.002 , for Fig. 4(a) and 4(b), respectively. We plot the dimensionless time-averaged normal stress $\bar{\sigma}_{zz}^* = \bar{\sigma}_{zz}/K_N$ against the imposed dimensionless shear rate $\dot{\gamma}^* = \dot{\gamma}d/\sqrt{K_N/\rho}$, where ρ is the mean mass density of the particles. Such dimensionless forms were pioneered by Campbell in his analyses on granular flows of soft particles using a linear contact model and various elasticity constants [27, 28]. Later these forms were adopted by Chialvo et al. [25], who rather focused on the role of the shear rate $\dot{\gamma}$ as we do in the present work. Following the scaling laws discovered by Chialvo et al. [25], we rescale both axes by factors $|\phi - \phi_c|^\nu$ such that $\nu = -1$ for $\bar{\sigma}_{zz}^*$ and $\nu = -4/3$ for $\dot{\gamma}^*$ in attempt to collapse the simulation results over various ϕ and material parameters. Two volume fractions (ϕ) are involved for

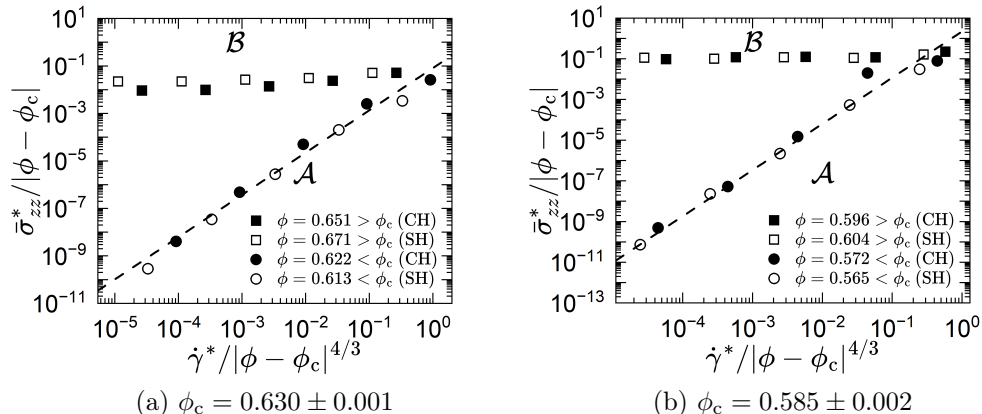


Figure 4: Time-averaged normal stresses $\bar{\sigma}_{zz}^* = \bar{\sigma}_{zz}/K_N$ versus shear rates $\dot{\gamma}^* = \dot{\gamma}d/\sqrt{K_N}/\rho$, both nondimensionalized, are acquired from the CH model (closed symbols) and the SH model (open symbols). (a) $\phi_c = 0.630 \pm 0.001$. $\mu_0 = 0.001$ for the CH model and $V_c = 6 \times 10^{-5}$ cm/s (with $\lambda_{SH} = 6 \times 10^{-7}$) for the SH model. (b) $\phi_c = 0.585 \pm 0.002$. $\mu_0 = 1.0$ for the CH model and $V_c = 6000$ cm/s (with $\lambda_{SH} = 60$) for the SH model. In each panel, the data are obtained with driving speeds from 0.01 cm/s up to 100 cm/s. After rescaled by $|\phi - \phi_c|^\nu$, the data in each panel are collapsed into two regimes: \mathcal{A} ($\phi < \phi_c$, circular symbols) represents collisional flows in which a dashed line is fitted to the data from the CH model; \mathcal{B} ($\phi > \phi_c$, square symbols) represents quasistatic flows in which $\bar{\sigma}_{zz}^*$ is almost independent of $\dot{\gamma}^*$. The slope of the dashed lines are 1.78 ± 0.08 and 2.27 ± 0.15 for the panels (a) and (b), respectively.

data from either the CH or the SH model. These data are collapsed into two regimes: Regime \mathcal{A} (with $\phi < \phi_c$) represents collisional flows, as the data fitting (dashed line) reveals scalings close to quadratic as $\bar{\sigma}_{zz}^* \propto \dot{\gamma}^{*2}$, implying the Bagnold scaling [29–31]. Regime \mathcal{B} (with $\phi > \phi_c$) represents quasistatic flows, such that the time-averaged normal stress is almost independent of the dimensionless shear rate $\dot{\gamma}^*$.

Figures 4(a) and 4(b) give two examples that, in terms of the time-averaged rheology, a granular packing governed by the SH model can be indistinguishable from that governed by the CH model. Despite the different values of ϕ for the CH and the SH model in each panel, these data points are all collapsed into the two regimes after the rescaling by the distance to the shared value of ϕ_c . This has confirmed that mapping the dynamics governed by the CH and SH model based on the distance to ϕ_c is indeed possible. On the other hand, Figs. 5(a) and 5(b) demonstrate that, with some certain

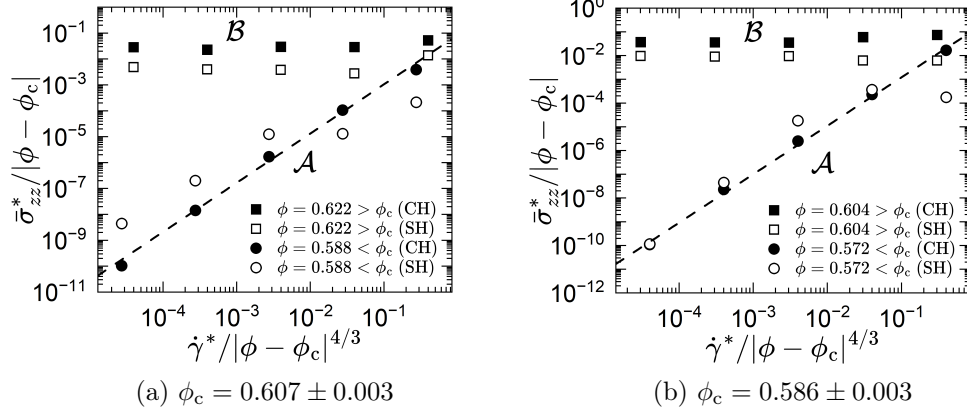


Figure 5: Same plot as Fig. 4 except with the choices of λ_{SH} that result in a clear departure from the data using the CH model, despite that ϕ_c being the same. (a) $\phi_c = 0.607 \pm 0.003$. $\mu_0 = 0.2$ for the CH model and $V_c = 0.06$ cm/s (with $\lambda_{\text{SH}} = 6 \times 10^{-4}$) for the SH model. (b) $\phi_c = 0.586 \pm 0.003$. $\mu_0 = 0.5$ for the CH model and $V_c = 0.6$ cm/s (with $\lambda_{\text{SH}} = 6 \times 10^{-3}$) for the SH model. The slope of the dashed lines are 1.90 ± 0.07 and 2.04 ± 0.05 for the panels (a) and (b), respectively.

values of λ_{SH} (varied by changing V_c), data of the SH model exhibit a clear deviation from those of the CH model, even with the similar values of ϕ_c and the same distance to these ϕ_c .

3.3. Time-averaged rheology and the temporal fluctuation

In order to gain insight into how the deviation from that of the CH model affect the macroscopic properties of the SH model, we further compare the rheological responses from both models. For a steady flow, it is common to characterize the rheology by expressing the stress ratio $\mu_{\text{eff}} \equiv \bar{\sigma}_{xz}/\bar{\sigma}_{zz}$ as a function of the inertial number $I \equiv \dot{\gamma}d/\sqrt{\bar{\sigma}_{zz}/\rho}$. Here, $\bar{\sigma}_{xz}$ (or $\bar{\sigma}_{zz}$) is the shear (or normal) stress on the wall and the bar stands for the time average. This ratio is often related to the inclination of the force chains relative to the boundaries [32–34]. In the conventional view (the CH model), at the low inertial number limit, the ratio is found to stay at a finite value that depends on the Coulomb coefficient μ_0 [26, 35]. Such $\mu_{\text{eff}}-I$ relationship is proved to be generic for both rigid [35] and soft particles [25, 36] under simple shear and other configurations [37].

Figure 6 demonstrates the case with $\phi_c = 0.630 \pm 0.001$ ($V_c = 6 \times 10^{-5}$ cm/s for the SH model and $\mu_0 = 0.001$ for the CH model) that is associated

with those data in Fig. 4(a). The graph shows a large collection of data with different combinations of $\dot{\gamma}$ and ϕ . Data from both models collapse on the same curve. In other words, the SH model and the CH model are indistinguishable in terms of the time-averaged rheology. And results from both models indicate a stable stress ratio (0.125) in the low inertial number limit.

For comparison, Fig. 7(a) demonstrates the case with $\phi_c = 0.607 \pm 0.003$ ($V_c = 0.06$ cm/s for the SH model and $\mu_0 = 0.2$ for the CH model) that is associated with those data in Fig. 5(a). It is worth noting that, for inertial numbers $I < 2 \times 10^{-2}$, the data from the SH model no longer overlap with those from the CH model. In other words, in the quasistatic regime, the dynamics governed by the SH model substantially changes from that of the CH model.

In Figs. 7(b) and 7(c), we plot the values of instantaneous stresses as functions of time extracted from the simulation data corresponding to the point α (governed by the SH model) and the point β (governed by the CH model) indicated by the arrows in Fig. 7(a); both are in the quasistatic regime. Figure 7(b) exhibits quasi-periodic growths and sudden drops of stresses, to which we refer as quaking [17]. In contrast, Fig. 7(c) shows relatively smooth curves and occasional small drops.

Comparing Figs. 7(b) and 7(c), we find that the typical magnitude of stresses in Fig. 7(c) is almost five times that of Fig. 7(b), even if their volume fractions are exactly the same. This suggests that the repeated reorganizations of particles (the quaking events in the SH simulations) have significantly weakened the granular packing.

3.4. State diagrams at different driving speeds

In Fig. 8, we present the state diagrams for granular packings governed by the SH model at three different driving speeds, $U = 0.01$ cm/s, 1.0 cm/s and 100 cm/s, respectively. (In our previous work [17], the granular packing was driven at $U = 0.1$ cm/s, with all other conditions identical to the present work.) The vertical and horizontal axes are respectively the volume fraction ϕ and the logarithm of the slipperiness $\dot{\gamma}d/V_c$ [17]. In this two-dimensional parameter space, the value of inertial number $I = \dot{\gamma}d/\sqrt{\bar{\sigma}_{zz}}/\rho$ is computed and color-coded like a heat map, based on various values of ϕ and V_c (across ten decades). The quaking regime is identified (and indicated by stripes) by observing the time sequence of the instantaneous coordination number,

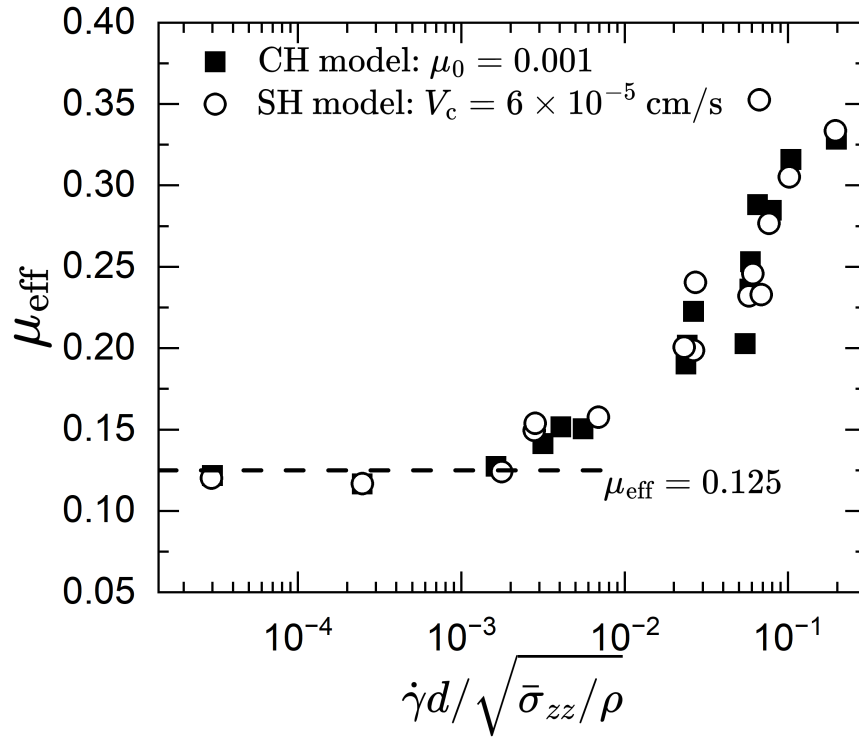
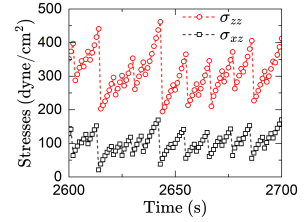
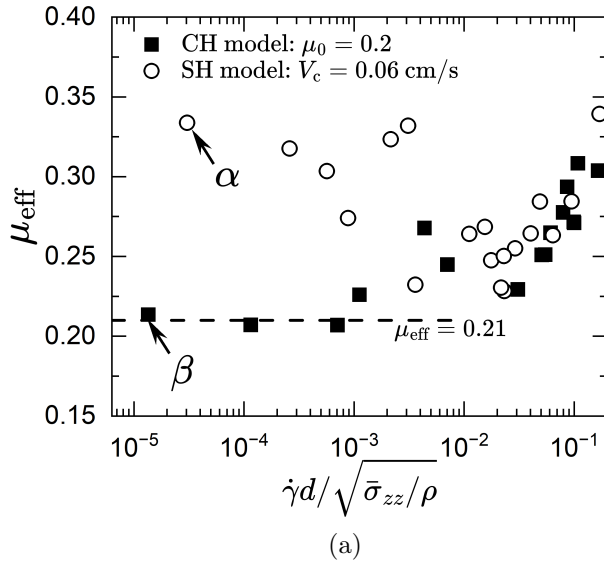
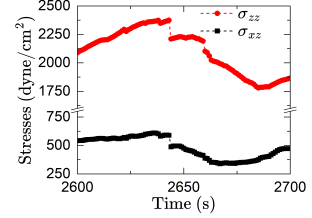


Figure 6: The stress ratio μ_{eff} plotted against the inertial number $I = \dot{\gamma}d/\sqrt{\bar{\sigma}_{zz}/\rho}$, for granular packings governed by the CH and the SH model, respectively, that share similar values of ϕ_c . $\phi_c = 0.630 \pm 0.001$, with $5.711 \times 10^{-4} \text{ s}^{-1} \leq \dot{\gamma} \leq 5.972 \text{ s}^{-1}$ and $0.613 \leq \phi \leq 0.641$. The dashed line indicates the stable stress ratio in the low inertial number limit. Both models exhibit identical rheological behavior over a wide range of I , as expected based on the universal behavior shown in Fig. 4(a).



(b) α , $I = 3.05 \times 10^{-5}$



(c) β , $I = 1.35 \times 10^{-5}$

Figure 7: (a) Same plot as Fig. 6 except that $\phi_c = 0.607 \pm 0.003$ with $4.994 \times 10^{-4} \text{ s}^{-1} \leq \dot{\gamma} \leq 5.711 \text{ s}^{-1}$ and $0.536 \leq \phi \leq 0.613$. While both models follow the same curve for $I > 2 \times 10^{-2}$, data from the SH model deviate substantially from the stable stress ratio (dashed line) at the low inertial number limit. Panels (b) and (c) are time sequences of the instantaneous stresses σ_{xz} and σ_{zz} extracted from the simulation data corresponding to points α and β in the panel (a), respectively. The deviation of the open circles in Panel (a) corresponds to the occurrence of quaking as shown in Panel (b).

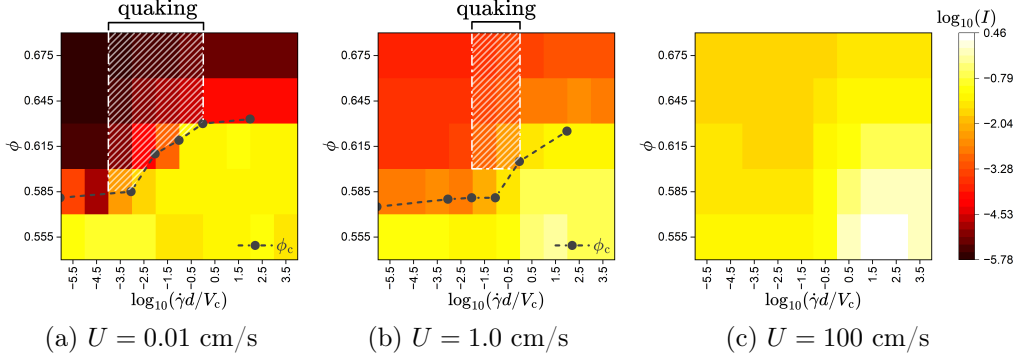


Figure 8: State diagrams for granular packings governed by the SH model, at three different driving speeds U . The data include simulations from thirteen different volume fractions ϕ but presented as five bins along the vertical direction. The horizontal coordinate is the logarithm of the slipperiness $\dot{\gamma}d/V_c$, generated from ten different values of V_c . The color shows the logarithm of the inertial number $I = \dot{\gamma}d/\sqrt{\bar{\sigma}_{zz}/\rho}$. In the panels (a) and (b), the closed circles indicate the locations of the critical volume fraction ϕ_c .

the elastic energy density, or the boundary stresses, since the occurrence of stick-slip fluctuations are consistent in time.

A very notable feature is that, as the value of U increases, the quaking regime suffers a shrinkage and eventually disappears from the parameter space. This can be perceived as the consequence of the increase of the inertial numbers: The entire parameter space eventually becomes collisional everywhere, so that the speed-dependent friction in the SH model can no longer produce the instability for triggering the quaking events. This is also consistent with Figs. 4 and 5, which show that the two *branches* (quasistatic versus collisional) are progressively merging as the shear rate increases. In Figs. 8(a) and 8(b), we have also indicated the location of ϕ_c . Note that the curve of ϕ_c also serves as the lower boundary of the quaking regime.

4. Discussion

In Sec. 3.1, we have interpreted λ_{SH} as the ratio of the retardation time $\tau_{\text{R}} = m\gamma_{\text{N}}/K_{\text{N}}$ to the critical weakening time $\tau_{\text{c}} = d/V_{\text{c}}$. Since these particles are characterized by the viscoelastic contact model Eq. (1), the elastic response in the normal direction between two colliding particles is not instantaneous but delayed, of which the timescale depends on γ_{N} . Specifically, our γ_{N} is sufficiently large such that the system is overdamped. Note that the

terms in the parentheses of Eq. (1) is analogous to the Kelvin-Voigt material, the simplest model for viscoelastic solids that is composed of a linear spring (characterized by the elastic modulus E) and a viscous damper (characterized by the viscosity η) linked in parallel [38]; this model is overdamped by nature as no inertial term is present. The Kelvin-Voigt material has only one characteristic timescale, $\tau_{KV} = \eta/E$.

In our SH model, the retardation time $\tau_R = m\gamma_N/K_N$ is analogous to τ_{KV} in the Kelvin-Voigt material. Essentially, τ_{KV} signifies how much time the Kelvin-Voigt material will take to reach the strain responding to a constant applied stress. Therefore, unless there is a network of enduring contacts ($\phi > \phi_c$), τ_R is a crude, simple estimate of the duration in which *two particles* transiently overlap while they are sliding with each other. On the other hand, when the sliding speed between two particles exceeding V_c , the critical weakening time τ_c is the longest time in which two overlapped particles sliding through a relative displacement equivalent to the mean diameter d . Therefore, one might expect that the velocity weakening should occur when $\lambda_{SH} \lesssim 1$. However, our results in Fig. 2(b) indicate a lower threshold down to the order of 10^{-2} . The reason behind such discrepancy remains elusive and requires further investigation in the future.

Also note that the resemblance of Figs. 2(a) and 2(b) by no means suggests that λ_{SH} is an apparent friction coefficient. By drawing the analogy between τ_R and τ_{KV} , we can see why λ_{SH} is relevant only close to ϕ_c by two conditions. First, the system must be overdamped. Particle collisions are underdamped when ϕ is far below ϕ_c ; in these scenarios the relevant timescale shall be the collision time [39] or simply $\dot{\gamma}^{-1}$.

Second, the overlapping is transient such that τ_R is relevant. The fluctuation of coordination numbers is at the peak when close to ϕ_c as shown in Fig. 1, suggesting frequent changes in overlapping between the neighboring particles. Once the force network is formed above ϕ_c , however, τ_R no longer represents the timescale of sliding due to the multiple, enduring overlaps per particle (i.e., sticking is dominant over sliding), and thus λ_{SH} is also irrelevant in such scenarios.

Finally, the two conditions suggest that ϕ_c of the SH model can substantially shift according to the choice of the contact model and the material parameters such as K_N , γ_N , and so on.

5. Summary and Concluding Remarks

In the present work with numerical simulations, we drive the granular packing beyond the quasistatic regime, and make detailed comparisons of results from the previously proposed Stribeck-Hertz model (SH, with a speed-dependent friction) and from the conventional Coulomb-Hertz model (CH, with a constant friction coefficient). The simulations from both models show that the values of the critical volume fraction ϕ_c are determined by the material parameters only, independent of the driving speed. Under both models in certain combinations of material parameters, the relationships between the mean normal stress and the shear rate can collapse if the differences between the volume fraction (ϕ) and the critical volume fraction (ϕ_c) are properly scaled. Meanwhile, we find that quaking is a distinct feature of the SH model: This is reflected by the anomalous stress ratio at low inertial numbers and the time sequences of instantaneous stresses. Investigations into the stress responses at various driving speeds make us conclude that the quaking occurs only in the intermediate range of slipperiness, in consistence with our previous work, but further reveal the progressive narrowing of the quaking regime and the disappearance of it at an extremely high shear rate.

From this work, we find that the volume fraction going above the critical volume fraction ϕ_c is a necessary condition for the quaking to occur. The effect of grain inertia generally suppresses the occurrence of quaking. And we expect that the ability to apply the SH model with the analysis of the critical volume fraction to a laboratory setting or field observations such as debris flows [24] will help us better understand the nature of granular flows in frictional grains.

References

- [1] Y. Ben-Zion, Collective behavior of earthquakes and faults: Continuum-discrete transitions, progressive evolutionary changes, and different dynamic regimes, *Reviews of Geophysics* 46 (2008) 2008RG000260. doi: [10.1029/2008RG000260](https://doi.org/10.1029/2008RG000260).
- [2] M. Bretz, R. Zaretski, S. B. Field, N. Mitarai, F. Nori, Broad distribution of stick-slip events in slowly sheared granular media: Table-top production of a gutenbergrichter-like distribution, *Europhysics Letters (EPL)* 74 (2006) 1116–1122. doi: [10.1209/epl/i2006-10048-2](https://doi.org/10.1209/epl/i2006-10048-2).

- [3] K. A. Dahmen, Y. Ben-Zion, J. T. Uhl, A simple analytic theory for the statistics of avalanches in sheared granular materials, *Nature Physics* 7 (2011) 554–557. [doi:10.1038/nphys1957](https://doi.org/10.1038/nphys1957).
- [4] L. de Arcangelis, C. Godano, J. R. Grasso, E. Lippiello, Statistical physics approach to earthquake occurrence and forecasting, *Physics Reports* 628 (2016) 1–91. [doi:10.1016/j.physrep.2016.03.002](https://doi.org/10.1016/j.physrep.2016.03.002).
- [5] G. Ma, Y. Zou, K. Gao, J. Zhao, W. Zhou, Size polydispersity tunes slip avalanches of granular gouge, *Geophysical Research Letters* 47 (2020) e2020GL090458. [doi:10.1029/2020GL090458](https://doi.org/10.1029/2020GL090458).
- [6] N. H. Sultan, K. Karimi, J. Davidsen, Sheared granular matter and the empirical relations of seismicity, *Physical Review E* 105 (2022) 024901. [doi:10.1103/PhysRevE.105.024901](https://doi.org/10.1103/PhysRevE.105.024901).
- [7] A. Petri, Statistics of intermittent granular flow from confined tabletop experiments, *La Rivista del Nuovo Cimento* 47 (2024) 353–396. [doi:10.1007/s40766-024-00055-y](https://doi.org/10.1007/s40766-024-00055-y).
- [8] Y. Ben-Zion, V. Lyakhovsky, Analysis of aftershocks in a lithospheric model with seismogenic zone governed by damage rheology, *Geophysical Journal International* 165 (2006) 197–210. [doi:10.1111/j.1365-246X.2006.02878.x](https://doi.org/10.1111/j.1365-246X.2006.02878.x).
- [9] G. D. Toro, R. Han, T. Hirose, N. D. Paola, S. Nielsen, K. Mizoguchi, F. Ferri, M. Cocco, T. Shimamoto, Fault lubrication during earthquakes, *Nature* 471 (2011) 494–498. [doi:10.1038/nature09838](https://doi.org/10.1038/nature09838).
- [10] K. Mizoguchi, T. Hirose, T. Shimamoto, E. Fukuyama, High-velocity frictional behavior and microstructure evolution of fault gouge obtained from nojima fault, southwest japan, *Tectonophysics* 471 (2009) 285–296. [doi:10.1016/j.tecto.2009.02.033](https://doi.org/10.1016/j.tecto.2009.02.033).
- [11] L. Wang, G. Kwiatek, E. Rybacki, A. Bonnelye, M. Bohnhoff, G. Dresen, Laboratory study on fluid-induced fault slip behavior: The role of fluid pressurization rate, *Geophysical Research Letters* 47 (2020) e2019GL086627. [doi:10.1029/2019GL086627](https://doi.org/10.1029/2019GL086627).

- [12] V. Rubino, N. Lapusta, A. J. Rosakis, Intermittent lab earthquakes in dynamically weakening fault gouge, *Nature* 606 (2022) 922–929. doi:[10.1038/s41586-022-04749-3](https://doi.org/10.1038/s41586-022-04749-3).
- [13] J.-C. J. Tsai, G.-H. Huang, C.-E. Tsai, Signature of transition between granular solid and fluid: Rate-dependent stick slips in steady shearing, *Physical Review Letters* 126 (2021) 128001. doi:[10.1103/PhysRevLett.126.128001](https://doi.org/10.1103/PhysRevLett.126.128001).
- [14] C.-E. Tsai, J.-C. J. Tsai, Dynamical force measurements for contacting soft surfaces upon steady sliding: Fixed-depth tribology, *Physical Review E* 109 (2024) 064802. doi:[10.1103/PhysRevE.109.064802](https://doi.org/10.1103/PhysRevE.109.064802).
- [15] B. Jacobson, The stribeck memorial lecture, *Tribology International* 36 (2003) 781–789. doi:[10.1016/S0301-679X\(03\)00094-X](https://doi.org/10.1016/S0301-679X(03)00094-X).
- [16] J. Williams, *Engineering Tribology*, Cambridge University Press, 2005. doi:[10.1017/CB09780511805905](https://doi.org/10.1017/CB09780511805905).
- [17] C.-E. Tsai, W.-C. Li, H.-C. Fan-Chiang, P.-Y. Hsiao, J.-C. Tsai, Two types of quaking and shear unjamming: State diagram for soft granular particles in quasistatic shear, *Physical Review Research* 6 (2024) 023065. doi:[10.1103/PhysRevResearch.6.023065](https://doi.org/10.1103/PhysRevResearch.6.023065).
- [18] A. P. Thompson, H. M. Aktulga, R. Berger, D. S. Bolintineanu, W. M. Brown, P. S. Crozier, P. J. in't Veld, A. Kohlmeyer, S. G. Moore, T. D. Nguyen, R. Shan, M. J. Stevens, J. Tranchida, C. Trott, S. J. Plimpton, Lammmps - a flexible simulation tool for particle-based materials modeling at the atomic, meso, and continuum scales, *Computer Physics Communications* 271 (2022) 108171. doi:[10.1016/j.cpc.2021.108171](https://doi.org/10.1016/j.cpc.2021.108171).
- [19] LAMMPS Documentation—Pair Styles: pair_style gran/hertz/history command, https://docs.lammps.org/pair_gran.html.
- [20] S. Ji, H. H. Shen, Internal parameters and regime map for soft poly-dispersed granular materials, *Journal of Rheology* 52 (2008) 87–103. doi:[10.1122/1.2807441](https://doi.org/10.1122/1.2807441).
- [21] D. Vescovi, S. Luding, Merging fluid and solid granular behavior, *Soft Matter* 12 (2016) 8616–8628. doi:[10.1039/C6SM01444E](https://doi.org/10.1039/C6SM01444E).

- [22] E. Aharonov, D. Sparks, Rigidity phase transition in granular packings, *Physical Review E* 60 (1999) 6890–6896. [doi:10.1103/PhysRevE.60.6890](https://doi.org/10.1103/PhysRevE.60.6890).
- [23] C. Song, P. Wang, H. A. Makse, A phase diagram for jammed matter, *Nature* 453 (2008) 629–632. [doi:10.1038/nature06981](https://doi.org/10.1038/nature06981).
- [24] R. Kostynick, H. Matinpour, S. Pradeep, S. Haber, A. Sauret, E. Meiburg, T. Dunne, P. Arratia, D. Jerolmack, Rheology of debris flow materials is controlled by the distance from jamming, *Proceedings of the National Academy of Sciences* 119 (2022) e2209109119. [doi:10.1073/pnas.2209109119](https://doi.org/10.1073/pnas.2209109119).
- [25] S. Chialvo, J. Sun, S. Sundaresan, Bridging the rheology of granular flows in three regimes, *Physical Review E* 85 (2012) 021305. [doi:10.1103/PhysRevE.85.021305](https://doi.org/10.1103/PhysRevE.85.021305).
- [26] D. Berzi, On granular flows: From kinetic theory to inertial rheology and nonlocal constitutive models, *Physical Review Fluids* 9 (2024) 034304. [doi:10.1103/PhysRevFluids.9.034304](https://doi.org/10.1103/PhysRevFluids.9.034304).
- [27] C. S. Campbell, Granular shear flows at the elastic limit, *Journal of Fluid Mechanics* 465 (2002) 261–291. [doi:10.1017/S002211200200109X](https://doi.org/10.1017/S002211200200109X).
- [28] C. S. Campbell, Granular material flows – An overview, *Powder Technology* 162 (2006) 208–229. [doi:10.1016/j.powtec.2005.12.008](https://doi.org/10.1016/j.powtec.2005.12.008).
- [29] R. A. Bagnold, Experiments on a gravity-free dispersion of large solid spheres in a newtonian fluid under shear, *Proceedings of the Royal Society of London. Series A. Mathematical and Physical Sciences* 225 (1954) 49–63. [doi:10.1098/rspa.1954.0186](https://doi.org/10.1098/rspa.1954.0186).
- [30] G. Lois, A. Lemaître, J. M. Carlson, Numerical tests of constitutive laws for dense granular flows, *Physical Review E* 72 (2005) 051303. [doi:10.1103/PhysRevE.72.051303](https://doi.org/10.1103/PhysRevE.72.051303).
- [31] Y. Forterre, O. Pouliquen, Flows of dense granular media, *Annual Review of Fluid Mechanics* 40 (2008) 1–24. [doi:10.1146/annurev.fluid.40.111406.102142](https://doi.org/10.1146/annurev.fluid.40.111406.102142).

- [32] M. E. Cates, J. P. Wittmer, J.-P. Bouchaud, P. Claudin, Jamming, force chains, and fragile matter, *Physical Review Letters* 81 (1998) 1841–1844. [doi:10.1103/PhysRevLett.81.1841](https://doi.org/10.1103/PhysRevLett.81.1841).
- [33] E. Aharonov, D. Sparks, Stick-slip motion in simulated granular layers, *Journal of Geophysical Research: Solid Earth* 109 (2004) 9306. [doi:10.1029/2003JB002597](https://doi.org/10.1029/2003JB002597).
- [34] D. Barreto, C. O’Sullivan, The influence of inter-particle friction and the intermediate stress ratio on soil response under generalised stress conditions, *Granular Matter* 14 (2012) 505–521. [doi:10.1007/s10035-012-0354-z](https://doi.org/10.1007/s10035-012-0354-z).
- [35] G. D. R. Midi, On dense granular flows, *The European Physical Journal E* 14 (2004) 341–365. [doi:10.1140/epje/i2003-10153-0](https://doi.org/10.1140/epje/i2003-10153-0).
- [36] Y. Gu, A. Ozel, S. Sundaresan, Rheology of granular materials with size distributions across dense-flow regimes, *Powder Technology* 295 (2016) 322–329. [doi:10.1016/j.powtec.2016.03.035](https://doi.org/10.1016/j.powtec.2016.03.035).
- [37] P. Jop, Y. Forterre, O. Pouliquen, A constitutive law for dense granular flows, *Nature* 441 (2006) 727–730. [doi:10.1038/nature04801](https://doi.org/10.1038/nature04801).
- [38] P. Hajikarimi, F. Moghadas Nejad, Mechanical models of viscoelasticity, in: *Applications of Viscoelasticity*, Elsevier, 2021, pp. 27–61. [doi:10.1016/B978-0-12-821210-3.00003-6](https://doi.org/10.1016/B978-0-12-821210-3.00003-6).
- [39] N. V. Brilliantov, F. Spahn, J.-M. Hertzsch, T. Pöschel, Model for collisions in granular gases, *Physical Review E* 53 (1996) 5382–5392. [doi:10.1103/PhysRevE.53.5382](https://doi.org/10.1103/PhysRevE.53.5382).